J Appl Electrochem (2011) 41:867–872
DOI 10.1007/s10800-011-0307-y

ORIGINAL PAPER

Photoelectrochemical characterization of the synthetic crednerite $CuMnO_2$

B. Bellal · B. Hadjarab · N. Benreguia · Y. Bessekhouad · M. Trari

Received: 18 December 2010 / Accepted: 25 March 2011 / Published online: 9 April 2011

Abstract High quality crednerite $CuMnO_2$ was prepared by solid state reaction at 950 °C under argon flow. The oxide crystallizes in a monoclinically distorted delafossite structure associated to the static Jahn–Teller (J–T) effect of Mn^{3+} ion. Thermal analysis showed that it converts reversibly to spinel $Cu_xMn_{3-x}O_4$ at ~420 °C in air and further heating reform the crednerite above 940 °C. $CuMnO_2$ is *p*-type, narrow semiconductor band gap with a direct optical gap of 1.31 eV. It exhibits a long-term chemical stability in basic medium (KOH 0.5 M), the semi logarithmic plot gave an exchange current density of 0.2 μA cm^{-2} and a corrosion potential of ~−0.1 V_{SCE}. The electrochemical oxygen insertion/desinsertion is evidenced from the intensity–potential characteristics. The flat band potential ($V_{fb} = -0.26$ V_{SCE}) and the holes density ($N_A = 5.12 \times 10^{18}$ cm^{-3}) were determined, respectively, by extrapolating the curve C^{-2} versus the potential to the intersection with $C^{-2} = 0$ and from the slope of the Mott–Schottky plot. From photoelectrochemical measurements, the valence band formed from Cu-3*d* wave function is positioned at 5.24 ± 0.02 eV below vacuum. The Nyquist representation shows straight line in the high frequency range with an angle of 65° ascribed to Warburg impedance originating from oxygen intercalation and compatible with a system under mass transfer control. The electrochemical junction is modeled by an equivalent electrical circuit thanks to the Randles model.

B. Bellal · N. Benreguia · Y. Bessekhouad · M. Trari (✉)
Laboratory of Storage and Valorization of Renewable Energies, Faculty of Chemistry, USTHB, BP 32, Algiers 16111, Algeria
e-mail: solarchemistry@gmail.com

B. Hadjarab
Laboratory of Solid Solutions, Faculty of Physic, USTHB, BP 32, Algiers 16111, Algeria

Keywords Crednerite · *p*-Type semiconductor · Photoelectrochemical · Nyquist plot

1 Introduction

The oxides are among the most stable materials for the water photo electrolysis [1, 2]. However, their performances are limited by either a wide forbidden band (E_g) exceeding 3 eV or a large electron affinity, attributed to a low lying valence band (VB) deriving mainly from O^{2-}: 2*p* orbital [3]. Hence, for small band gap semiconductors (SCs), the conduction band (CB) is located at insufficient negative potential to liberate hydrogen with appreciable rates. Our research program consists of developing new optically materials for photoelectrochemical (PEC) applications [4, 5]. Coupling a small gap E_g with a low electron affinity should theoretically result in VB of cationic parentage with a small gap [6]. d^{10} configuration may be used for this purpose, and encouraging results have been yet made regarding to the photo-to-chemical energy conversion over $Cu^{+}M^{3+}O_2$ typified by the mineral delafossite $CuFeO_2$ [7], where M is commonly 3*d*-metal or a rare earth. The introduction of Cu: 3*d*-levels make the electronic bands independent of pH, thus minimizing the losses resulting from H_2 and O_2 over-voltages. $CuMO_2$ may be important in many engineering aspects like photo voltaic devices [8, 9], photocatalytic reactions [10], and more recently environmental protection [11].

Among the congeners, the crednerite $CuMnO_2$ was first reported as a two-dimensional structure by Kondrachev [12]. The detailed crystal structure was elucidated from powder with the space group C2/m and confirmed later on the single crystal [13]. The unit cell shows a monoclinic distortion

associated with Jahn–Teller (J–T) effect of Mn^{3+} ($3d^4$) supporting the finding of two longer (0.2260 nm) and four shorter distances (0.1929 nm). On the other hand, the flat band potential (V_{fb}) does not vary significantly with pH and the electronic bands can be suitably adjusted to redox couples in solution. We have taken advantage of this property and at basic pHs, CB is located at potential more cathodic than the H_2O/H_2 level, and $CuMnO_2$ has been tested successfully as hydrogen photocathode [14]. However, whereas the physical properties of $CuMnO_2$ are little known [15], no previous studies on detailed PEC characterization have been reported. The transport properties may be modified by substitution of suitable cations. We have examined various aspects of the solid solution $Cu_{1+x}Mn_{1-x}O_2$ with the presence of two J–T ions, i.e., Mn^{3+} and Cu^{2+} [16] and this was undertaken to enhance the electrical conductivity. In a previous article, we reported the physical properties of $CuMnO_2$ prepared by $Cu^+ \rightarrow Li^+$ exchange reaction [17]. In continuation, this study covers the optical and PEC properties of $CuMnO_2$ prepared by solid state reaction under O_2 free atmosphere. A lot of information can be obtained from the electrochemical impedance spectroscopy (EIS) which are useful to correlate the transport properties to the morphology of the material. The conductivity depends on both the bulk and the grain boundaries and the contribution can be resolved by exploiting the responses when one applies AC signal to the junction at variable frequencies. The data allow modeling the electrochemical junction $CuMnO_2$/KOH electrolyte by an equivalent electrical circuit.

2 Experimental

$CuMnO_2$ was synthesized from stoichiometric amounts of binary oxides MnO and CuO (prefired at 400 °C) both of purity >99.9%. The starting mixture was thoroughly mixed in an agate mortar and heat treated in an alumina boat at 960 °C under pure Ar flow. Two grindings and firings were required to achieve a well-crystallized oxide. High purity argon was further deoxygenated by flowing over a bed of iron fillings at 500 °C. The end product exhibits a dark brown color and was identified by X-ray diffractometry (XRD) using Ni-filtered Cu Kα radiation. The data were recorded for 10 s at each 0.02° step over the 2θ interval 10°–100°. The lattice constants were refined from corrected peaks position with a least square program. The density was determined from the method of hydrostatic weighting in toluene. The thermal analysis (TGA) was performed in air at a heating rate of 3 °C min^{-1} using a computer-controller thermo balance Setaram (Setsys 16/18). The oxidation state of copper was determined iodometrically by dissolving the oxide under inert atmosphere in HCl (4 N) with KI excess. The liberated iodine has been accurately titrated with NaS_2O_3. 80% density was obtained by sintering pressed pellets at 980°. The gap E_g was obtained by application of the Munk Kubelka equation of the diffuse reflectance spectrum. The resistivity was measured by the two probe method under argon atmosphere using a current 1 mA.

Electrical contact with copper wires was made onto unexposed surface of pellets with conductive silver paint. Then, the pellets were enrobed in glass holders with epoxy resin. The polarization curves were plotted in a three-electrode electrochemical set up. A large area Pt electrode (Tacussel) served as auxiliary electrode, and all the potentials were given with respect to a saturated calomel electrode (SCE) and monitored by a voltalab PGZ301 potentiostat (Radiometer). The electrolyte (KOH, 0.5 M) was continually flushed with nitrogen, and the working electrode was illuminated through an optical window by a 650 W halogen lamp (Dyr, General Electric). The point of zero charge (*pzc*) has been accurately determined by measuring the equilibrium pH of an aqueous solution containing a suspension of powdered oxide. The capacitance was determined as a function of the potential with a rate of 10 mV $step^{-1}$. The complex impedance data, recorded at the free potential obtained from the open circuit potential (OCP), were acquired using small amplitude wave signals with a frequency response analyzer in the range (10^{-3}–10^5 s^{-1}). The solutions have been prepared from reagents of analytical grade quality and doubly distilled water.

3 Results and discussion

Chemical analysis indicates that the oxide is composed of 52.11 wt. % of Mn_2O_3 and 47.89 wt% of Cu_2O, a composition very close to the theoretical one (respectively 52.46 and 47.54 wt%). The oxidation state of copper, determined by iodometric titration, shows a slight deviation from the stoichiometry, leading to the formula $CuMnO_{2.01}$. The XRD pattern (Fig. 1), virtually free from secondary phases, is successfully indexed in a monoclinic symmetry (space group: C2/m) associated with J–T Mn^{3+} ion. All the peaks are assigned to the crednerite phase in agreement with the JCPDS card No 50-0860. The measured density (5.10 g cm^{-3}) agrees with that calculated on the basis of two formula weights per unit cell (5.34 g cm^{-3}). TGA plot of $CuMnO_2$ (Fig. 2) exhibits a weight gain at 435 °C due to oxidation and which results in the reversible transition into oxygen rich spinel:

$$(3-x)\ CuMnO_2 + 0.5\ O_2 \rightarrow Cu_xMn_{3-x}O_4 + (3-2x)\ CuO \qquad (1)$$

The maximal gain at 620 °C accounting for 5.36% of the initial mass corresponds to the formation of $Cu_xMn_{3-x}O_4$

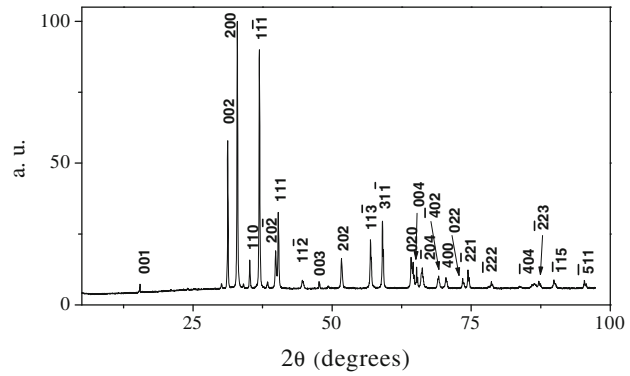

Fig. 1 X-ray diffraction pattern of $CuMnO_2$

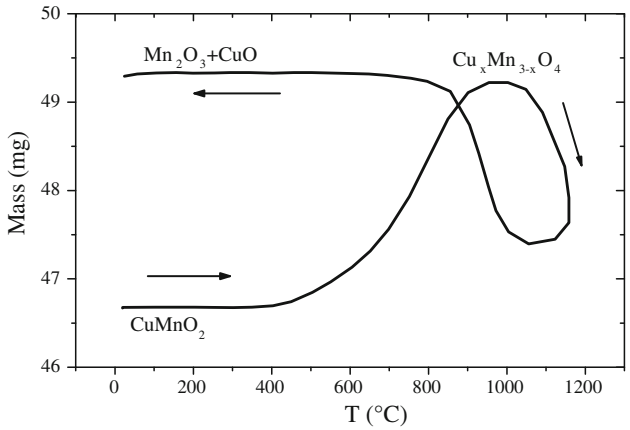

Fig. 2 Combined TGA curve of $CuMnO_2$ performed in air

($x = 1.02$). The reduction of the spinel begins at 940 °C and leads to the reformation of $Cu_{1.1}Mn_{0.9}O_2$. This composition has been determined by interpolation from a constructed calibration plot of the lattice constants a and c as a function of the composition x in $Cu_{1+x}Mn_{1-x}O_2$ [12]. Both a and c increase linearly with composition ($0 \leq x \leq 0.20$) following the Vegard's law and this means that the solid solution $Cu_{1+x}Mn_{1-x}O_2$ is a substitutional system throughout the whole composition range. At 1154 °C, the crednerite melts peritectically, and XRD analysis indicated the coexistence of the cubic spinel phase and CuO/Cu_2O. The irreversible conversion is confirmed by the absence of peaks on the reverse scan. The situation looks similar to that observed with $CuFeO_2$ that converts reversibly to the spinel at ~500 °C [18]. It is worth while to note that under argon flow, no weight change was observed in the TGA plot.

The crednerite structure contains layers of MnO_6 octahedra sharing common edges. The Cu-3d-orbital splits into a filled d-level (VB) of about 2 eV above the O^{2-}-2p orbital and empty level which forms CB, some 5.5 eV above O^{2-}-2p orbital. The effective gap refers to the transition of these levels, due to the separation between the non bonding t_{2g} orbital and hybridized 4s/3d orbital and is

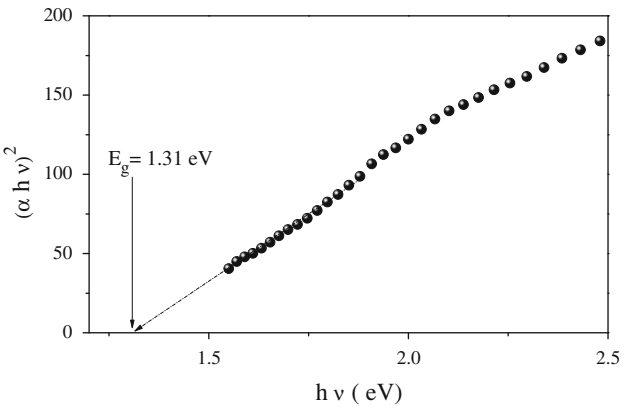

Fig. 3 Determination of the direct allowed transition in $CuMnO_2$

reduced to approximately 1.4 eV because of the low ionicity of the Mn–O bond. This electronic structure gives the oxide its semi conductivity [15] and is compatible with the chemical stability. The plots $(\alpha h\nu)^{1/n}$ versus $h\nu$ should be linear with intercepts equal to the interband transition energies, the exponent n depends on the type of transition; $n = 2$ for indirect allowed and $n = ½$ for direct allowed transition. The extrapolation of $(\alpha h\nu)^2$ to $h\nu$ axis gives a direct transition at 1.31 eV (Fig. 3).

Goodenough [19] as proposed a critical intercation distance for 3d electrons, above which localized behavior is expected. The Cu–Cu length, equal to b-parameter, is longer than that in copper (0.127 nm)[1] and $CuMnO_2$ is expected to be SC. A large anisotropy is common in the crednerite, and the pellet consists of randomly oriented microcrystal. The charge-compensating process, due to oxygen insertion in the 2D framework, maintains the electro neutrality by inducing Cu^{2+} formation. The electrical conductivity is thermally activated (Fig. 4) and follows an Arrhenius-type law ($\sigma = \sigma_o e^{-E\sigma/RT}$). Frequency dependence of AC conductivity shows that the conduction occurs by electrons hopping among localized sites with average activation energy (E_σ) of 0.11 eV, in conformity with small polaron hopping. The holes move in narrow VB of Cu-3d orbital leading to a low mobility μ_h (2.18×10^{-6} cm^2 V^{-1} s^{-1}),[2] responsible of the weak photocurrent (see below). Such value is close to that observed over isotypic delafossites [20].

In the electrochemistry of SCs, the corrosion is important to investigate owing to its negative aspect for PEC applications. The dissolution rate of $CuMnO_2$ increases approximately linearly in a logarithm scale with decreasing pH. Long-term chemical stability was carried out up to 2 months of continuous operation in neutral solution (Na_2SO_4 0.1 M) and the corrosion rate, determined from

[1] Calculated for copper crystallizing in face-centered cubic with a lattice constant of 0.3615 nm.

[2] Determined from the formula $\sigma = e\ \mu_h\ N_A$.

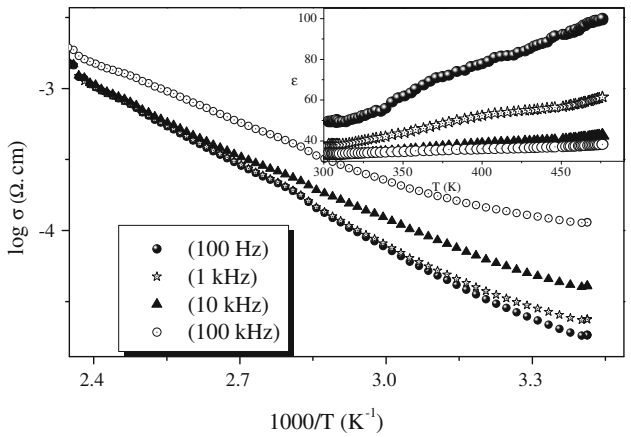

Fig. 4 Logarithm of conductivity versus reciprocal temperature for $CuMnO_2$ at various frequencies. *Insert*: the corresponding dielectric constants

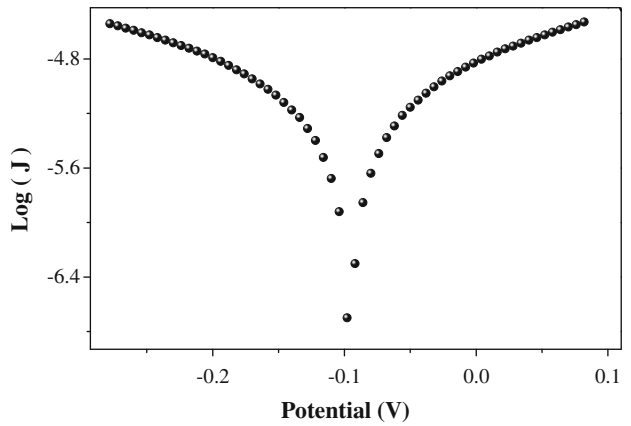

Fig. 5 Semi-logarithmic plot of $CuMnO_2$ in Na_2SO_4 (0.5 M) solution

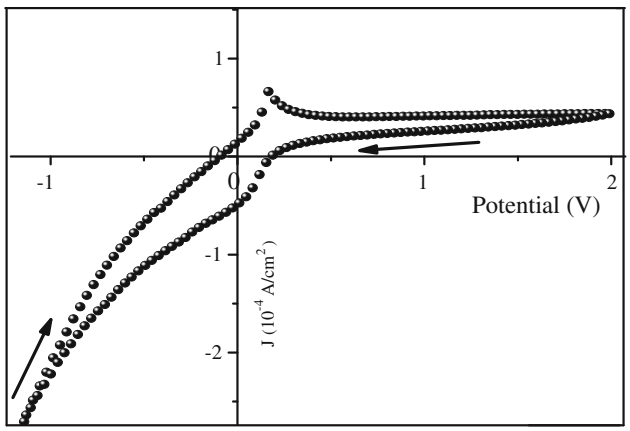

Fig. 6 Typical cyclic $J(V)$ characteristic of $CuMnO_2$ electrode in KOH (0.5 M) solution under N_2 bubbling (scan rate at 2 mV s^{-1})

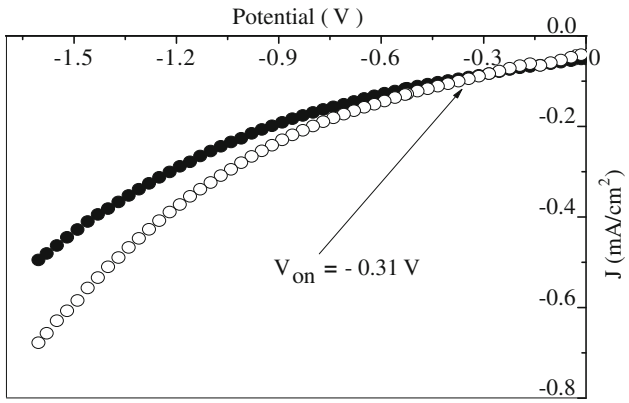

Fig. 7 The $J(V)$ characteristics of $CuMnO_2$ in KOH (0.5 M) solution in the dark (*filled circle*) and under illumination (*open circle*)

dissolved copper, was found to be only 0.14 μmol month^{-1}. Such result is supported by the semi logarithmic plot which is a common technique for examining the corrosion process (Fig. 5). A long lived electrode should have a small exchange current density J_0 and a low Tafel slope $\partial \log J/\partial V$. A density J_0 of 0.2 μA cm^{-2}, a corrosion potential of −0.1 V, and a polarization resistance of 10.74 kΩ cm^2 confirm the chemical stability. The current J_0 is best though as the rate constant of the electron transfer at zero potential. The electrochemical behavior of $CuMnO_2$ in KOH (0.5 M) solution shows an anodic peak at ∼0.17 V (Fig. 6) due to an internal redox process, i.e., oxygen intercalation in the layered lattice with concomitant Cu^+ oxidation according to the reaction:

$$CuMnO_2 + 2\delta OH^- \rightarrow CuMnO_{2+\delta} + \delta H_2O + 2\delta e^- \quad (2)$$

where δ stands for the amount of incorporated oxygen. The quantity of electricity under the peak is evaluated to 0.48 mC cm^{-2} and this charge corresponds approximately to the oxidation of 3.3×10^{15} at. Cu^+ cm^{-2}. The peak at ∼0 V, on the reverse scan, is due to the reversible reduction of $Cu^{2+/+}$ followed subsequently by oxygen desinsertion.

A direct relationship is evident between the photo catalytic performance and the energetic position of the electronic bands, determined from the photocurrent onset potential (V_{on}). The photocurrent J_{ph} starts to flow at −0.31 V and increases progressively along the negative-going polarization with no saturation (Fig. 7). The rather slow increase of J_{ph} is characteristic of *p*-type conductivity with a low recombination process of electron/hole (e^-/h^+) pairs and the quality factor. Below −1 V, J_{ph} is superimposed to H_2 evolution (gas bubbles are noticeable on the electrode). This result shows that Cu^{2+} ions act as acceptors, as it could be expected. If cathodically stable, *p*-type material must have a corrosion potential more negative than CB. A small decrease of the dark current is observed which indicates a slow transfer of excess holes in conformity with the low mobility. In the absence of surface states, the potential V_{on} can be reasonably likened to the flat band

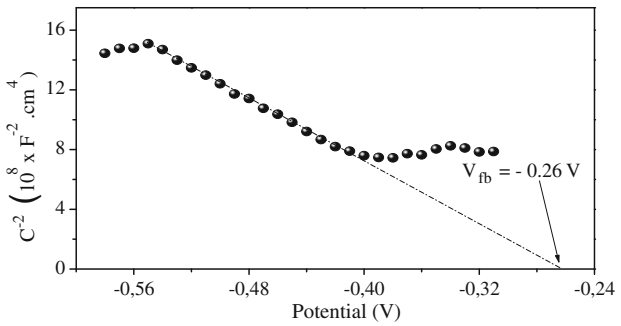

Fig. 8 The Mott–Schottky representation of $CuMnO_2$ in KOH (0.5 M) solution at a frequency of 1 kHz

potential (V_{fb}). In general, the difference ($V_{fb} - V_{on}$) decreases with increasing the light intensity. Changing the pH of the solution in the range (7–14) made no difference in the potential V_{on} and the shiftless of V_{on} with pH is attributed to the non adsorption of ions (e.g., H^+, OH^-). However, the potential V_{fb} value has been accurately determined from the interfacial capacitance:

$$C^{-2} = -(2/e\varepsilon\varepsilon_0 N_A)\{V - V_{fb} - kT/e\} \quad (3)$$

where all the symbols have their usual significations. The potential V_{fb} (−0.26 V) is determined from the cross point of the extended plot to potential axis. The small discrepancy between the potentials V_{on} and V_{fb} is attributed to the absence of sub band gap states within the gap region. The linear plot ($C^{-2} - V$) (Fig. 8) indicates a constant holes density N_A (5.12×10^{18} cm^{-3}) that characterizes non degenerate semi conductivity and a broad space charge region:

$$\delta = \left(\frac{2\varepsilon\varepsilon_0(V_{fb} - V)}{eN_A}\right)^{0.5} \quad (4)$$

The width δ (23 nm), calculated for a band bending ($V_{fb} - V$) of 0.5 V, extends over many repeat crystallographic units. The dielectric constant ($\varepsilon \sim 50$) was determined on sintered pellets (Fig. 4 Inset). The transition to the plateau region in the $C^{-2}(V)$ curve below −0.5 V indicates a change from a charges accumulation to depletion state where the electronic bands are flattened out. The density of acceptors is by two orders of magnitude lower than that derived from the chemical analysis (2×10^{20} cm^{-3}) and this indicates a trapping of surface holes in surface-polaron states. The potential V_{fb} gives the position of VB with respect to vacuum:

$$P = E^0 + eV_{fb} + E_\sigma + 0.056(\text{pH} - pzc) \quad (5)$$

where E^0 (=4.75) is the free energy of the electron versus SCE. Therefore, the P value, (5.24 ± 0.2 eV) below vacuum, is typical of transition metal oxides in which VB is made up of 3*d* wave function.

$CuMnO_2$ is relatively a new oxide, and it is instructive to predict its theoretical electro affinity (EA_{theo}). The electron affinity is defined as the energy required removing an electron from the CB to vacuum. A correlation exists between EA_{theo}, the electro negativity (χ) and E_g[3]:

$$EA_{theo.} = \left[\chi Cu \chi Mn \chi O^2\right]^{1/4} - 0.5E_g \quad (6)$$

The *pzc* (=10.75) is the pH at which the net charge of adsorbed ions onto the surface is zero and it is the only value for which the meaningful EA_{theo} can be evaluated. EA_{theo} (4.21 eV) is typical of oxides in which CB is made up of 3*d* orbital [15]. The discrepancy between EA_{exp} (3.93 eV = $P - E_g$) and EA_{theo} indicates that the above relation gives rather a rough approximation of the electron affinity of SC compounds.

The impedance data, collected in the frequency range (10^{-3} to 10^5 Hz) at the free potential, provide insights of the electrical processes which regulate the charge transfer at the interface (Fig. 9). The absence of semi circle in the Nyquist representation eliminates the grain boundaries contribution. The slope of the line gives information about the type of diffusion. A linear region inclined to an angle of 65° indicates that a diffusion process, known as Warburg impedance (Z_W) is involved, i.e., O^{2-} moves through the layered lattice and the system is under mass transfer control with one time constant. This indicates that the kinetic of interfacial exchange tends to be faster (decreasing R) and the impedance becomes dominated by the intercalation process owing to the slowness of oxygen insertion. The diffusional control is more pronounced due to the layered nature of $CuMnO_2$ which facilitates the mass transport but not enough to compete with the interfacial exchange. This experiment clearly evidences the low mobility of oxygen in the $CuMnO_2$ lattice which does not migrate easily if one refers to low diffusion coefficient D_{ox}, a behavior explained in part by the high ionic radius of oxygen (0.14 nm). From electrochemical measurements on isotypic oxides, D_{ox} was found to be $\sim 10^{-16}$ cm^2 s^{-1} [21]. We also note a slight offset near the origin indicating a low series resistance attributed to the KOH ionic conductor (2.35 Ω cm^2).

The curvature at low frequencies in the Bode plot, i.e., the variation of the imaginary part of the impedance Z with frequency (Fig. 9 Inset) confirms the diffusion process. The plateau region at high frequencies is due to the existence of a space charge region (*Rp*). In the limit of fast interfacial charge transfer and low intercalation, the impedance takes the form which is similar to that expected for purely

[3] For an element, χ is the arithmetic mean of EA and the first ionization energy.

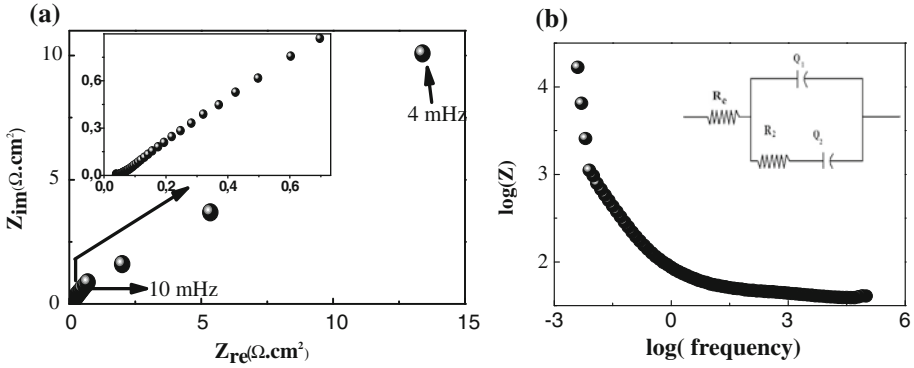

Fig. 9 **a** Complex impedance plot of $CuMnO_2$ in KOH (0.5 M) solution. *Inset*: the high frequencies region. **b** The Bode diagram measured at the free potential E_{free} after 30 min of immersion. *Inset*: the equivalent electrical circuit

resistive response. A change in the slope is observed at 1 mHz suggesting blocking electrode behavior. We recall that the frequency decreases as we go to the right hand side. The barrier is modeled as double layer over the grains region, and the data are analyzed by fitting to an equivalent electrical circuit thanks to a Randles model (Fig. 9 Inset).

4 Conclusion

Our research is oriented to the development of new semi conducting materials for PEC applications with a high reducing ability, i.e., CB of cationic parentage. For this purpose, a d^{10} configuration may be used and we successfully prepared a new manganate. The crednerite $CuMnO_2$ showed a monoclinically distorted structure attributed to the J–T effect of Mn^{3+}. The oxide displays a semi conducting behavior evidenced from the cathodic photocurrent. The conductivity obeys to an Arrhenius-type law where most holes are localized on Cu^{2+} surface-polarons states. $CuMnO_2$ is chemically stable over a fair pH range, absorbs more sunlight, and is promising for bias-free photocathode. Both the valence and the CBs are of cationic character and pH insensitive, compatible with the chemical stability. The absence of arc in the complex impedance agrees with a negligible effect of grains boundaries to the electrical conduction; the high frequency straight line is attributed to the oxygen insertion followed by an inclination due to the blocking behavior. An electrical equivalent circuit is proposed to simulate the electrochemical behavior.

Acknowledgments We thank Dr A. Louafi for helpful discussion regarding the EIS interpretation and Dr M. Kebir for assistance in obtaining the X-ray powder data. Financial support was provided by the Faculty of Chemistry (Algiers).

References

1. Bellal B, Hadjarab B, Bouguelia A, Trari M (2009) Theor Exp Chem 45:172
2. Alam KM, Yang OB (2009) Catal Today 146(1):177
3. Stroyuk AL, Kryukov AI, Kuchmii SYa, Pokhodenko VD (2009) Theor Exp Chem 45:209
4. Brahimi R, Bessekhouad Y, Bouguelia B, Trari M (2007) Catal Today 122:62
5. Rajeshwar K (2007) J Appl Electrochem 37:765
6. Trari M, Bouguelia B, Bessekhouad Y (2006) Sol Energy Mater Sol Cells 90:190
7. Dordor P, Chaminade JP, Wichainchai A, Marquestaut E, Doumerc JP, Pouchard M, Hagenmuller P (1988) J Solid State Chem 75:105
8. Guranathan K, Baeg JO, Mi Lee S, Subramanian E, Moon SJ, Kong KJ (2003) Catal Commun 9:395
9. Barnabé A, Mugnier E, Presmanes L, Tailhades Ph (2006) Mater Lett 60(29):3468
10. Dong H, Li Z, Xu X, Ding Z, Wu L, Wang X, Fu X (2009) Appl Catal B 89:551
11. Omeiri S, Gabès Y, Bouguelia A, Trari M (2008) J Electroanal Chem 614:31
12. Kondrashev ID (1959) Sov Phys Crystallogr 3:703
13. Töpfer J, Trari M, Gravereau P, Chaminade JP, Doumerc JP (1995) Z Kristallogr 210:184
14. Bessekhouad Y, Trari M, Doumerc JP (2003) Int J Hydrog Energy 28:43
15. Doumerc JP, Trari M, Töpfer J, Fournès L, Grenier JC, Pouchard M, Hagenmuller P (1994) Eur J Solid State Inorg Chem 31:705
16. Trari M, Töpfer J, Dordor P, Grenier JC, Pouchard M, Doumerc JP (2005) J Solid State Chem 178:2751
17. Bessekouad Y, Gabes Y, Bouguelia A, Trari M (2007) J Mater Sci 42(15):6469
18. Lalanne M, Barnabé A, Mathieu F, Thailhades Ph (2009) Inorg Chem 48:6065
19. Goodenough JB (1983) In: Procceding in the second European conference on solid state chemistry, Veldhoven, the Netherlands
20. Bellal B, Saadi S, Koriche N, Bouguelia A, Trari M (2009) J Phys Chem Solids 70(7):1132
21. Brahimi R, Trari M, Bouguelia A, Bessekhouad Y (2010) J Solid State Electrochem 14:1333